ACS APPLIED MATERIALS & INTERFACES

Research Article

www.acsami.org

Engineering $Zn_{1-x}Cd_xS$/CdS Heterostructures with Enhanced Photocatalytic Activity

Kui Li,[‡,†] Rong Chen,[‡,†] Shun-Li Li,[‡] Shuai-Lei Xie,[‡] Long-Zhang Dong,[‡] Zhen-Hui Kang,[*,§] Jian-Chun Bao,[*,‡] and Ya-Qian Lan[*,‡]

[‡]Jiangsu Key Laboratory of Biofunctional Materials, School of Chemistry and Materials Science, Nanjing Normal University, Nanjing 210023 Jiangsu P. R. China

[§]Jiangsu Key Laboratory for Carbon-based Functional Materials and Devices, Institute of Functional Nano and Soft Materials (FUNSOM), Soochow University, Suzhou 215123, P. R. China

Supporting Information

ABSTRACT: Various porous $Zn_{1-x}Cd_xS$/CdS heteorostructures were achieved via in situ synthesis method with organic amines as the templates. Because of the larger radius of Cd^{2+} than that of Zn^{2+}, CdS quantum dots are formed and distributed uniformly in the network of $Zn_{1-x}Cd_xS$. The $Zn_{1-x}Cd_xS$/CdS heterostructure with small Cd content (10 at %) derived from ethylenediamine shows very high H_2-evolution rate of 667.5 μmol/h per 5 mg photocatalyst under visible light ($\lambda \geq 420$ nm) with an apparent quantum efficiency of 50.1% per 5 mg at 420 nm. Moreover, this $Zn_{1-x}Cd_xS$/CdS heterostructure photocatalyst also shows an excellent photocatalytic stability over 100 h.

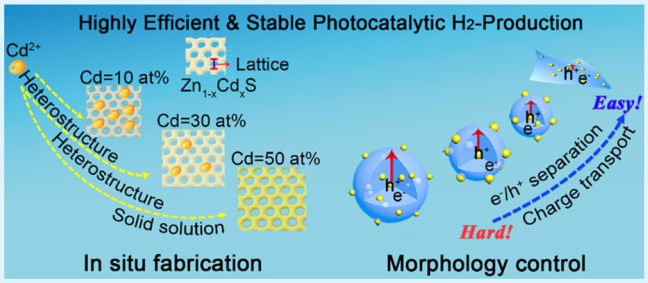

KEYWORDS: *$Zn_{1-x}Cd_xS$/CdS, heterostructure, CdS quantum dots, in situ synthesis, photocatalytic activity*

1. INTRODUCTION

Constructing the semiconductor heteronanomaterials has become a popular design strategy for improving photocatalytic and optical properties in photocatalyst and luminescent devices.[1−6] Up to date, most of the heterostructure photocatalyst are formed in at least two steps via fabricating one semiconductor on the surface of another one,[7] which decreases the amount of active sites and restricts the scale-up fabrication.[4] Also, the heterostructure always bears the poor lattice and band structure matching due to the distinct intrinsic parameters of the different semiconductors.[8−10] Solid-state solution-based semiconductor heterostructure can relieve the interface stress derived from the lattice mismatch and optimize the band structure matching because of the tunable lattice constant and band structure of solid solution.[11] As the "alloy" of ZnS and CdS, $Zn_{1-x}Cd_xS$ solid solution possesses continuously tunable lattice constant ranging from 0.331 (⟨100⟩ of ZnS) to 0.359 nm (⟨100⟩ of CdS) and bandgap (E_g) ranging from 3.66 (ZnS) to 2.4 eV (CdS).[11−13] Notably, $Zn_{1-x}Cd_xS$ solid solution shows better photocatalytic activity than that of single CdS and the CdS loaded with Pt as cocatalyst.[11] Thus, the heterojunction of $Zn_{1-x}Cd_xS$/CdS should be a promising photocatalyst with good visible-light absorption and high spatial separation efficiency of charge carriers.[7] So far, typical fabrication method of $Zn_{1-x}Cd_xS$ solid solution includes coprecipitation,[14] chemical bath deposition,[15] cation exchange,[7] wet chemistry,[16] and thermolysis method.[11] Compared with the thermolysis method,[11] the wet chemistry method is convenient and simple, but it still bears poor control on the band structure of $Zn_{1-x}Cd_xS$ and requires long reaction time owing to the larger radius of Cd^{2+} (0.97 Å) than that of Zn^{2+} (0.74 Å).[7,11,16,17] Moreover, the design and in situ synthesis of $Zn_{1-x}Cd_xS$ based heterojunction ($Zn_{1-x}Cd_xS$/CdS) as photocatalyst is rarely reported.

Herein, we report the in situ synthesis of various porous $Zn_{1-x}Cd_xS$/CdS heteorostructures by regulating the ratio of Cd/Zn with organic amines (ethylenediamine, EDA; 1,2-diaminopropane, DAP; 3,3′-diaminodipropylamine, DADPA) as the templates. Because of the larger radius of Cd^{2+} than that of Zn^{2+}, CdS quantum dots (CdS QDs) formed and distributed uniformly in the network of $Zn_{1-x}Cd_xS$ showed extremely important role for improving the spatial separation/transport efficiency of charge carriers.[5,18] The optimal $Zn_{1-x}Cd_xS$/CdS heterostructure with small Cd content (10 at%) derived from EDA shows very high H_2-evolution rate of 667.5 μmol/h per 5 mg of photocatalyst under visible light ($\lambda \geq 420$ nm), corresponding to an apparent quantum efficiency equaling to 50.1% per 5 mg at 420 nm. Moreover, this $Zn_{1-x}Cd_xS$/CdS heterostructure photocatalyst also shows a good stability over 100 h. Here, the in situ formed $Zn_{1-x}Cd_xS$/CdS heterostructure

Received: March 4, 2016
Accepted: May 12, 2016
Published: May 12, 2016

ACS Publications © 2016 American Chemical Society

DOI: 10.1021/acsami.6b02765
ACS Appl. Mater. Interfaces 2016, 8, 14535−14541

and highly porous morphology are responsible for the substantially improved photocatalytic activity.

2. EXPERIMENTAL SECTION

Sample Preparation. The inorganic−organic hybrid nanomaterial was prepared using $ZnCl_2$, $Cd(NO_3)_2{\cdot}4H_2O$, and CH_4N_2S as Zn, Cd, S precursors, and different amines as solvents. In a typical synthesis, 1.5 mmol of $ZnCl_2$ and $Cd(NO_3)_2{\cdot}4H_2O$ with different Cd/(Zn+Cd) molar ratios, and 3 mmol of thiourea were dissolved in 30 mL of pure amine solvent under ultrasound until all the reagents were dissolved. The solution was then transferred into a 50 mL Teflon-lined autoclave and maintained 180 °C for 21 h. The final yellow products were rinsed three times with distilled water and ethanol, respectively, and dried at 60 °C for overnight in a vacuum oven to evaporate the solvent ethanol. Thirty mg as-prepared hybrid nanomaterial was dissolved in 12.8 mL deionized water under ultrasound for a few minutes. After several minutes, the obtained solutions were transferred into 15 mL autoclaves and maintained at 140 °C for 12 h. The final products were respectively rinsed with distilled deionized water and ethanol for three times, and dried at 60 °C overnight in the vacuum oven to evaporate the solvent ethanol. The samples with different Cd content derived from EDA were postannealed at 500 °C for 1 h with a ramping rate of 5 °C/min in nitrogen atmosphere to remove the CdS phase. The $Zn_{1-x}Cd_xS$ with different Cd content were prepared via thermolysis method according to the previous publication.[11] The detail experimental procedure could be found in the Supporting Information.

Characterization. X-ray diffraction (XRD) patterns were recorded on a D/max 2500 VL/PC diffractometer (Japan) equipped with graphite monochromatized Cu Kα radiation (λ = 1.54060 Å). The transmission electron microscopy (TEM) and high-resolution TEM (HRTEM) images were recorded on JEOL-2100F apparatus at an accelerating voltage of 200 kV. The morphology was investigated by a field emission scanning electron microscope (SEM, JSM-7600F) at an acceleration voltage of 10 kV. Element content analysis was tested on an inductively coupled plasma (ICP) spectroscope (Prodigy, Leeman, America). UV−Vis diffused reflectance spectra were recorded using a Cary 5000 UV−vis spectrometer (Viarian, USA) with $BaSO_4$ as a reflectance standard. The Brunauer−Emmett−Teller (BET) specific surface area (S_{BET}), nitrogen adsorption and water vapor adsorption of the heterojunction samples were analyzed by an Autosorb-iQ adsorption apparatus (Quantachrome instruments, USA). The BET surface area was determined by a multipoint BET method using adsorption data in the relative pressure (P/P_0) range of 0.05−0.3. A desorption isotherm was used to identify the pore size distribution via the Barret−Joyner−Halender (BJH) method, assuming a cylindrical pore model. Electrochemical impedance spectroscopy (EIS) measurements were conducted from 200 kHz to 100 mHz with an amplitude of 10 mV at the open-circuit voltage on the electrochemical station (Bio-Logic SP-150) by a three-electrode system in 0.1 M Na_2S+0.02 M Na_2SO_3 solution under a surface power density of about 0.1 mW/cm^2. Samples were performed on the glassy carbon electrode (GCE, 3 mm in diameter) as the working electrode, a saturated calomel electrode (SCE) as the reference electrodes and a Pt wire as the counter electrode. Two milligrams of the catalysts were dispersed in 1 mL distilled water by sonication to form a homogeneous ink. Typically, 5 μL of well-dispersed catalysts were covered on the glassy carbon electrode and then dried in an ambient environment for measurements.

Photocatalytic Hydrogen Production. The photocatalytic H_2-production experiments were performed via a photocatalytic H_2-production activity evaluation system (CEL-SPH2N, CEAULight, China) in a 300 mL Pyrex flask, and the openings of the flask were sealed with silicone rubber septum. A 300 W xenon arc lamp through a UV-cutoff filter with a wavelength range of 420−800 nm. The focused intensity on the flask was about 200 mW·cm^{-2}. In a typical photocatalytic H_2-production experiment, 5 mg of the prepared photocatalyst was suspended in 100 mL of mixed solution containing Na_2S (0.35 M) and Na_2SO_3 (0.25 M). Before irradiation, the system was vacuumed for 5 min via the vacuum pump to completely remove the dissolved oxygen and ensure the reactor was in an anaerobic condition. The evolved H_2 content was analyzed by gas chromatography. The photocatalytic stability was performed using the similar parameters to the evaluation of photocatalytic activity. To evaluate the recycling performance and eliminate the effect of the decreased content of sacrificial agent, we collected and tested the sample by renewing the sacrificial agent every 20 h. The apparent quantum efficiency (AQE) of 5 mg of catalyst for H_2 evolution is measured using a 420 ± 8 nm band-pass filter. The average intensity of irradiation is determined to be 10.13 mW cm^{-2} by an FZ-A visible-light radiometer. The number of incident photon is 7.84×10^{20}, and the AQE for H_2 evolution is calculated as 50.1% according to the following equation[12]

$$\mathrm{QE} = \frac{2{\cdot}\text{the number of evolved } H_2 \text{molecules}}{\text{the number of incident photons}}$$

3. RESULTS AND DISCUSSION

Similar to the fabrication of $Zn_{1-x}Cd_xS$ solid solution,[12,13,17,19] the $Zn_{1-x}Cd_xS$/CdS heterostructure was fabricated via an in situ wet-chemistry process. The porous heterostructure sample with Cd content of only 10 at% (abbreviated as ZCS0.1) was fabricated using organic EDA as template. Characterizations of $Zn_{1-x}Cd_xS$/CdS heterostructure in ZCS0.1 via XRD, UV−vis diffuse reflection spectra, TEM and HRTEM were exhibited in Figure 1. The comparison results of XRD patterns for ZCS0.1,

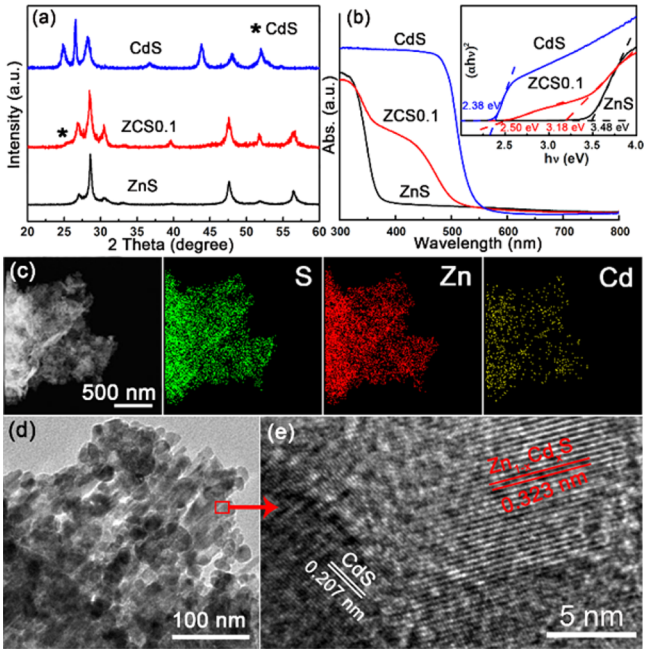

Figure 1. Characterization of the $Zn_{1-x}Cd_xS$/CdS heterostructure. (a) The comparison results of the XRD patterns, (b) UV−vis absorption spectra and $(\alpha h\nu)^2$ versus $h\nu$ curve (inset) of ZnS, ZCS0.1 and CdS derived from EDA. (c) Element mapping, (d) TEM morphology, and (e) HRTEM images of ZCS0.1.

ZnS and CdS derived from EDA (Figure 1a) indicate the obvious CdS phase in ZCS0.1. Compared with the XRD pattern of $Zn_{0.9}Cd_{0.1}S$ prepared via thermolysis method (Figure S1),[11] the diffraction peaks corresponding to $Zn_{1-x}Cd_xS$ phase in ZCS0.1 shift to the right side dramatically, indicating the less Cd amount in its solid solution than that of $Zn_{0.9}Cd_{0.1}S$ (9 at %),[3] although the Cd content in ZCS0.1 is 10.75 at % from the

DOI: 10.1021/acsami.6b02765
ACS Appl. Mater. Interfaces 2016, 8, 14535−14541

ICP result (Figure S2). This inconsistency indicates the remnant Cd^{2+} in ZCS0.1 exists in the form of CdS.

Investigation of the band structure of ZnS, ZCS0.1, and CdS via UV−vis absorption spectra (Figure 1b) indicates that the band edge of ZCS0.1 shifts to much longer wavelength than that of ZnS. As can be observed from the inset, ZCS0.1 shows very close E_g in the visible region to that of CdS. This result is totally different from that of the previously reported $Zn_{0.9}Cd_{0.1}S$ prepared via thermolysis method because of the existence of the CdS phase.[11] It is noteworthy that ZCS0.1 shows two band edges in UV and visible region, corresponding to the absorption of $Zn_{1-x}Cd_xS$ and CdS,[7] respectively. Moreover, both ZCS0.1 and the corresponding hybrid sample without the second processing step at 140 °C ($ZCS0.1(en)_{0.5}$) show the exactly same E_g value (Figure S3), confirming the in situ synthesis of $Zn_{1-x}Cd_xS$/CdS heterostructure. The elemental mapping images (Figure 1c) imply that all the elements distribute evenly in the entire skeleton of ZCS0.1. Characterization of the microstructure morphology of ZCS0.1 via TEM suggests its irregular nanosheet morphology (Figure 1d). Two lattice fringes corresponding to $Zn_{1-x}Cd_xS$ and CdS can be observed from HRTEM of ZCS0.1 (Figure 1e), which further confirms the existence of $Zn_{1-x}Cd_xS$/CdS heterostructure.

To investigate the formation mechanism of $Zn_{1-x}Cd_xS$/CdS heterostructure, and the effect of Cd content on the phase structure, microstructure and photocatalytic activity of the samples derived from EDA, a series of samples with nominal Cd/(Cd+Zn) molar ratio n are obtained and labeled as ZCSn (n = 0, 0.1, 0.3, 0.5, 0.7, 0.9, and 1). The XRD patterns of the as-prepared samples with different amount of Cd were compared with that of the solid solution samples prepared by thermolysis method in Figure 2a. An increased hexagonal phase of $Zn_{1-x}Cd_xS$ can be observed in the samples derived from EDA with increasing concentration of Cd. Compared with the $Zn_{1-x}Cd_xS$ with the same amount of Cd prepared via thermolysis method,[11] the diffraction peaks corresponding to $Zn_{1-x}Cd_xS$ in ZCS0.1 and ZCS0.3 shift to the right side dramatically, indicating the less amount of Cd in their solid solution. Notably, the obvious CdS phase can be found in ZCS0.1 and ZCS0.3. Moreover, the diffraction peaks of $Zn_{1-x}Cd_xS$ phase in ZCS0.5 also shift slightly in comparison with $Zn_{0.5}Cd_{0.5}S$, which may be result from the composition fluctuation as reported in previous publication,[20] whereas ZCS0.7 shows the exactly same diffraction peaks positions to that of $Zn_{0.3}Cd_{0.7}S$ solid solution prepared via thermolysis method.

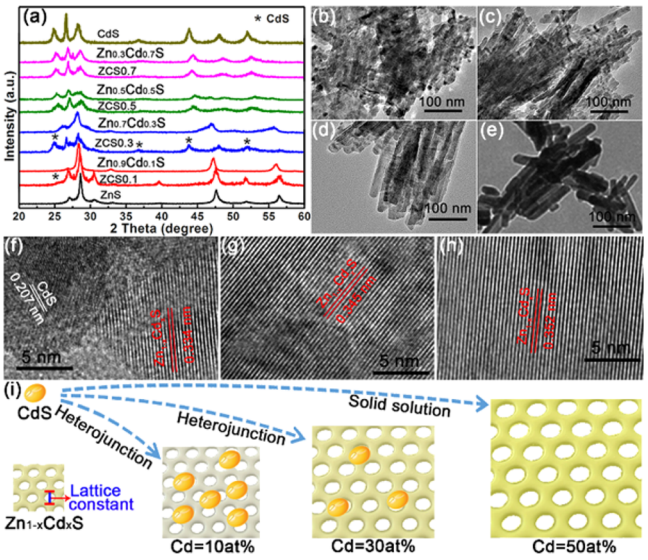

Figure 2. (a) Comparison results of the X-ray diffraction patterns of the samples derived from EDA with different amount of Cd to that of the solid solution prepared with thermolysis method; TEM photograph of (b) ZCS0.3, (c) ZCS0.5, (d) ZCS0.7, and (e) CdS derived from EDA; HRTEM images of (f) ZCS0.3, (g) ZCS0.5, and (h) ZCS0.7; (i) scheme illustrating the formation mechanism of $Zn_{1-x}Cd_xS$/CdS heterostructure via regulating the ratio of Cd/Zn at low process temperature.

The transmission electron microscope (TEM) images of these samples indicate that the samples with elevated Cd content show obvious nanosheet morphology owing to the nanorod microstructure of CdS (Figure 2b−e). The effect of Cd amount on the UV−vis diffuse reflection spectra of the as prepared samples is displayed in Figure S4. It can be observed that the band edge of the samples shifts to longer wavelength with increasing amount of Cd. Significantly, all the samples with Cd content ranging from 10 to 70 at % show the similar E_g. This result is absolutely different from that of the previously reported $Zn_{1-x}Cd_xS$ prepared via the thermolysis method due to the existence of CdS phase in the samples with small Cd content. Moreover, the slightly higher E_g in ZCS0.1 and ZCS0.3 than that in CdS may be attributed to the quantum size effect of CdS.[7] Effect of Cd content on the phase structure of the as-prepared samples is confirmed by HRTEM (Figure 2f−h). In contrast to the $Zn_{1-x}Cd_xS$/CdS heterostructure in ZCS0.1 and ZCS0.3, no lattice fringes corresponding to CdS were observed in ZCS0.5 and ZCS0.7. The composition of these samples was confirmed by ICP spectrum, and no remarkable variations in Cd/(Zn+Cd) ratio were observed in these samples (Figure S2).

It is well-known that the wet chemistry method bears poor control on the band structure of $Zn_{1-x}Cd_xS$ and requires long reaction time owing to the larger radius of Cd^{2+} than that of Zn^{2+}.[11,16] Significantly, this shortcoming of wet chemistry method could make the in situ synthesis of $Zn_{1-x}Cd_xS$/CdS heterojunction possible, especially for the sample with small Cd amount. As shown in the proposed mechanism of the formation of $Zn_{1-x}Cd_xS$/CdS heterostructure in the samples with different ratios of Cd/Zn (Figure 2i), the in situ formation of $Zn_{1-x}Cd_xS$/CdS heterostructure was achieved by carefully regulating the ratio of Cd/Zn. During the low temperature wet-chemistry process, the Zn^{2+}, Cd^{2+}, and S^{2-} are apt to form solid solution and CdS phases, with the CdS entering into the lattice of solid solution gradually in longer reaction time. For the sample with small Cd content, it is very difficult for the further reaction between CdS and $Zn_{1-x}Cd_xS$, whereas $Zn_{1-x}Cd_xS$ with larger Cd content possesses a larger lattice constant and then CdS can enter into its lattice easily.

Large surface area, which provides more exposed active sites and decreases the transmission distance of photoexcited electron/hole pairs, is required for the highly efficient photocatalysts. Additionally, water vapor adsorption is another important factor for improving the photocatalytic activity. Nitrogen and water vapor adsorption/desorption isotherms of the samples are demonstrated in Figure 3a, b, respectively. Increasing Cd amount in the samples leads to a dramatic decrease in their nitrogen adsorption, S_{BET} and water vapor adsorption, and ZCS0.1 possesses the highest S_{BET} and water vapor adsorption volume stemming from its nanosheet

DOI: 10.1021/acsami.6b02765
ACS Appl. Mater. Interfaces 2016, 8, 14535−14541

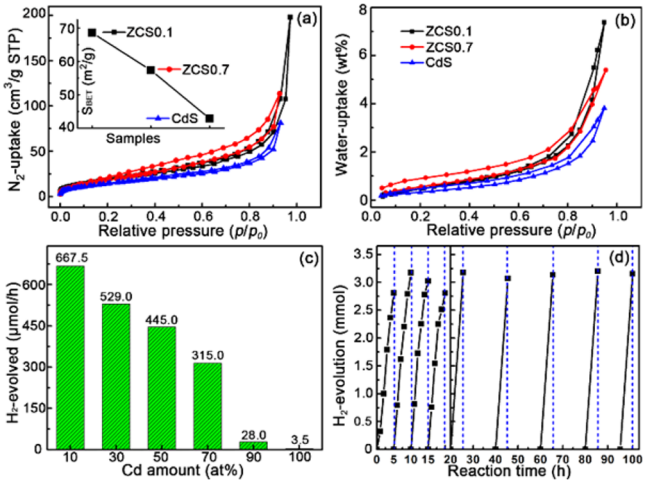

Figure 3. (a) Nitrogen (S_{BET} is exhibited as inset), (b) water vapor adsorption/desorption isotherms and (c) the visible light photocatalytic H_2-production activity of the samples with different amount of Cd derived from EDA. (d) Photocatalytic stability of ZCS0.1 in mixed solution containing Na_2S (0.35 M) and Na_2SO_3 (0.25 M).

morphology. This nanosheet morphology could exhibit more exposed heterostructure active sites, and consequently facilitate the separation, transport, and utilization efficiency of the photogenerated electron/hole pairs.[21−26]

The visible-light photocatalytic H_2-evolution activity of the as-prepared samples with different Cd contents is compared in Figure 3c. In contrast to the negligible visible-light photocatalytic activity of pure ZnS, the sample with only 10 at % Cd (ZCS0.1) shows extremely high H_2-evolution rate due to its $Zn_{1-x}Cd_xS$/CdS heterojunction and large S_{BET}. However, a further increase in the Cd content in the samples led to a slight deterioration of the photocatalytic activity as a result of the decreased amount of CdS QDs, and ZCS0.1 shows the maximum H_2-evolution activity of 667.5 μmol/h per 5 mg photocatalyst and an excellent AQE of 50.1% per 5 mg at 420 nm. This photocatalytic activity exceeds that of CdS derived from EDA and deionized water by more than 181 and 1211 times respectively (Figure S5). Moreover, this result is very competitive compared to the other CdS-based photocatalytic nanomaterials (Table S1).[3,4,10,19,27−33]

The well-dispersed CdS QDs in the highly porous $Zn_{1-x}Cd_xS$ nanosheet skeleton is responsible for the improved photocatalytic activity.[18] Moreover, ZCS0.1 shows outstanding photocatalytic stability over 100 h (Figure 4d). Additionally, the crystal structure of the ZCS0.1 shows no obvious change after the photocatalytic reaction, and the ZCS0.1 after the photocatalytic stability testing also shows the nanosheet morphology (Figure S6), indicating the excellent stability of the ZCS0.1.

To investigate the effect of solvent templates on the microstructure and photocatalytic H_2-production activity of the heterostructure samples, we adopted different solvents including DAP, DADPA, and deionized water (DIW) to fabricate $Zn_{1-x}Cd_xS$/CdS heterostructure with the optimal amount of Cd using the same processing parameters with the samples derived from EDA. These samples were abbreviated as ZCS-DAP, ZCS-DADPA, and ZCS-DIW, respectively. The ball-and-stick models of the different types of solvent are exhibited in Figure 4a. In contrary to DIW solvent, the amine solvents could connect with the reactant and form inorganic−

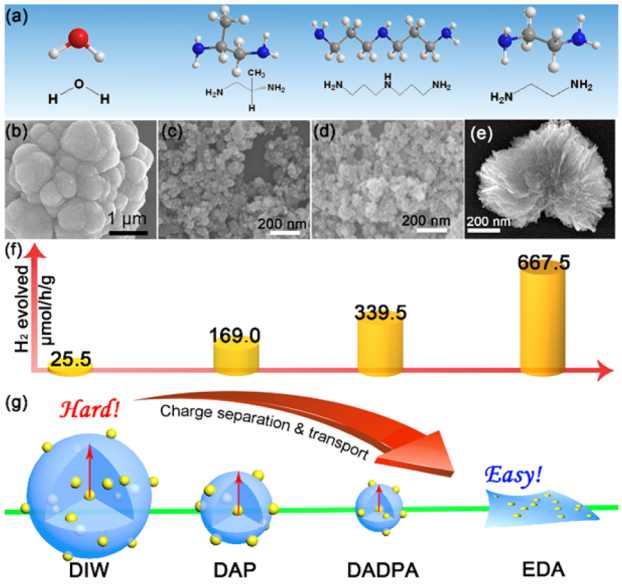

Figure 4. (a) Ball-and-stick models of the different types of solvent. The SEM images of the samples derived from (b) DIW, (c) DAP, (d) DADPA, and (e) EDA. (f) Photocatalytic H_2-production activity of the samples with different amount of Cd under visible-light ($\lambda \geq 420$ nm) irradiation. (g) The scheme illustrating the effect of microstructure morphology on the separation and transport efficiency of photogenerated charge carriers.

organic hybrid nanomaterial. Consequently, the microstructure of the samples derived from amine solvents can be tuned by the molecular structure of these organic amines. The reactant-EDA could interconnect with each other and form the nanosheet morphology because of its suitable length of molecular chain. However, the branched chain in DAP and the much longer length of chain in DADPA facilitate the formation of nanoparticles morphology. As demonstrated in the scanning electron microscope (SEM) images of the samples derived from different types of solvent, the ZCS-DADPA, ZCS-DAP and ZCS-DIW are nanoparticles morphology with different diameters (Figure 4b−d), whereas ZCS0.1 shows the flowerlike microstructure assembled with nanosheets (Figure 4e). The composition of the samples prepared with different types of solvent is confirmed by ICP spectrum (Figure S7). ZCS-DIW shows a larger ratio of Cd/(Zn+Cd) than 10 at %, which may be attributed to the incomplete reaction stemming from its larger radius.

Characterization of the phase structure of the samples derived from different solvents via XRD (Figure S8a) indicates that ZCS-DAP and ZCS-DADPA possess stronger CdS phase than that of ZCS0.1. As shown in the UV−vis absorption spectra (Figure S8b), the samples derived from the different solvents show the similar band edge and E_g to that of ZCS0.1. The different microstructure of the heterojunction samples derived from different templates affect their nitrogen adsorption as well as S_{BET} dramatically (Figure S9). ZCS-DADPA possesses larger S_{BET} than that of ZCS-DAP due to its smaller particle size. It is noteworthy that the distinct microstructure brings about the drastically different H_2-production activity (Figure 4f). The heterostructure sample derived from EDA possesses the maximum photocatalytic H_2-evolution activity due to its nanosheet microstructure. Additionally, the larger diameter of nanoparticle in the samples

DOI: 10.1021/acsami.6b02765
ACS Appl. Mater. Interfaces 2016, 8, 14535−14541

derived from DIW than those derived from, DAP and DADPA decreases its H_2-production rate dramatically.

Effect of different morphologies derived from different types of solvent on the charge transport/separation efficiency and photocatalytic activity of the samples is exhibited in Figure 4g. It is well-known that only the charge carriers on the surface of the photocatalyst can contribute to the improvement of photocatalytic activity. The transport distance and the number of exposed active sites are very important for improving separation and transport efficiency of electron/hole pairs.[2,14] ZCS0.1 shows the shortest transport route than that of the samples with sphere microstructure derived from DAP, DADPA, and DIW. The transport distance of ZCS-DIW, ZCS-DAP, and ZCS-DADPA decreased with their reductive diameter. Correspondingly, the relative order of photocatalytic H_2-evolution rate for the samples was found to be ZCS0.1 > ZCS-DADPA > ZCS-DAP > ZCS-DIW. The electrochemical impedance spectra (EIS) analysis (Figure S10) further affirmed that ZCS0.1 shows the fastest interfacial electron transfer than that of ZCS-DAP and ZCS-DIW.

To further confirm the important role of $Zn_{1-x}Cd_xS$/CdS heterojunction for improving photocatalytic activity of the samples derived from EDA, we adopted a postannealing process at 500 °C under pure a N_2 atmosphere to deal with the samples with different amounts of Cd. The corresponding samples were abbreviated as ZCSn-500. ZCS0.1−500 shows the similar microstructure (Figure 5a), S_{BET} and the ratio of

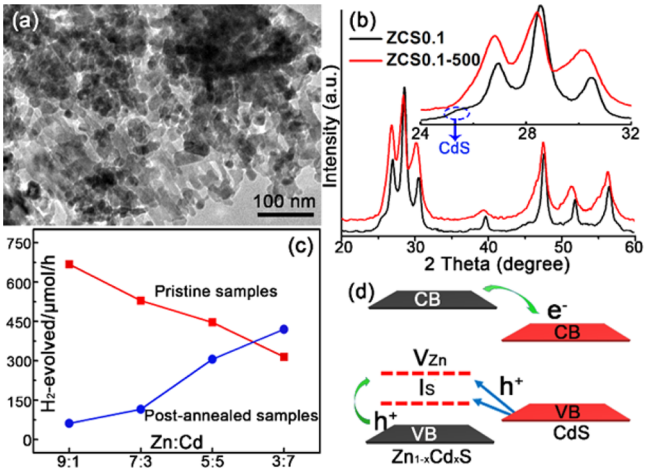

Figure 5. Effect of postannealing process at 500 °C on the (a) TEM image, and (b) the XRD patterns of ZCS0.1. (c) Effect of postannealing process on the photocatalytic H_2-evolution activity the samples with different amount of Cd, and (d) the schematic illustrating the transport and separation of photogenerated charge carriers in $Zn_{1-x}Cd_xS$/CdS heterostructure.

Cd/(Zn+Cd) (Figure S11a, b) to that of ZCS0.1. Although both the shifts of diffraction peak position and band edge from XRD (Figure 5b) and UV−vis diffuse reflection spectra (Figure S11c), respectively, indicate the disappearance of CdS phase, which is further confirmed by the HRTEM (Figure S11d). As shown in Figure S12, the photocatalytic H_2-production rate of ZCS0.1 decreased for 90.8% after the postannealing process owing to the disappearance of $Zn_{1-x}Cd_xS$/CdS heterostructure. Thanks to its nanosheet morphology, ZCS0.1−500 shows much higher photocatalytic activity than that of $Zn_{0.9}Cd_{0.1}S$ prepared by thermolysis method. The interfacial electron transfer of ZCS0.1, ZCS0.1−500 and porous CdS is further confirmed by EIS (Figure S13).[34] ZCS0.1 shows the smallest semicircle in the middle-frequency region, indicating its fastest interfacial electron transfer.

Effects of postannealing process on the phase structure, microstructure and photocatalytic activity in samples with different amount of Cd derived from EDA were investigated systematically. The samples ranging from ZCS0.1 to ZCS0.7 exhibit similar microstructure before and after the postannealing process (Figure S14a−d). A dramatic variation in XRD patterns and band structure in ZCS0.1−500 and ZCS0.3−500 can be observed from Figure S14e−i. Whereas, ZCS0.7 shows no variation of bandgap and diffraction peak position after the postannealing process. Moreover, all the samples dealt with the postannealing process show similar S_{BET} (Figure S14j) to that of pristine samples. As shown in Figure 5c, the photocatalytic H_2-evolution rate of ZCS0.1−500 decrease more dramatically (90.8%) than that of ZCS0.3−500 (78.3%) with respect to that of the pristine samples owing to the larger amount CdS in ZCS0.1. ZCS0.5 exhibits a slight decrease of 31.4% (Figure S14k), which may be attributed to the disappearance of composition fluctuation. Notably, ZCS0.7−500, possessing pure solid-solution phase, shows larger photocatalytic H_2-production rate than ZCS0.7 because of its improved crystallinity after the postannealing process at high temperature.

It was extensively reported that the localized acceptor states (V_{Zn} and I_S) in ZnS may act as the means of the transfer of photoexcited holes from the CdS to the ZnS.[4,35,36] Moreover, $Zn_{1-x}Cd_xS$ possesses the similar peak position of the emission derived from the local acceptor states (such as V_{Zn}) and does not change with increasing amount of the Cu^{2+} dopant, indicating their constant energy levels of the negative defect states with respect to the conduction band.[37,38] The defect states related acceptor levels in ZnS and ZCS0.1 were investigated by the photoluminescence (PL) spectra (Figure S15). ZCS0.1 shows the similar peak position (around 426 nm) of the emission derived from V_{Zn} to that of ZnS, which is similar to the previous reports.[9,36,37] Based on the above experimental results, the proposed charge transfer and separation mechanism in $Zn_{1-x}Cd_xS$/CdS heterojunction is exhibited in Figure 5d. The photoexcited holes from CdS transported into the local acceptor states in $Zn_{1-x}Cd_xS$, and the photogenerated electrons from CB of $Zn_{1-x}Cd_xS$ transferred to the CB of CdS. Moreover, as the localized acceptor states (such as V_{Zn}) is higher than that of the VB of CdS, the photogenerated holes in the VB of $Zn_{1-x}Cd_xS$ solid solution transferred to the its acceptor states. This spatial separation of the photogenerated electron/hole pairs could dramatically inhibit their recombination and increase the utilization efficiency of charge carriers. Consequently, the heterostructure sample fabricated via an in situ method exhibits much larger photocatalytic hydrogen production activity than that of solid solution samples.

4. CONCLUSION

In summary, porous $Zn_{1-x}Cd_xS$/CdS heterostructures were synthesized using different organic amines as the templates by an in situ synthesis method through carefully regulating the ratio of Cd/Zn. These $Zn_{1-x}Cd_xS$/CdS heterostructures show excellent visible-light H_2-evolution activity; and the sample with 10 at% Cd derived from EDA shows the best H_2-production rate of 667.5 μmol/h per 5 mg photocatalyst with AQE of about 50.1% per 5 mg at 420 nm. Moreover, this $Zn_{1-x}Cd_xS$/CdS heterostructure shows outstanding photocatalytic stability

DOI: 10.1021/acsami.6b02765
ACS Appl. Mater. Interfaces 2016, 8, 14535−14541

over a period of 100 h. This study may open a new general route for the design of photocatalyst with improving photocatalytic activity and stability based on the semiconductor heterostructures.

■ ASSOCIATED CONTENT

Supporting Information

The Supporting Information is available free of charge on the ACS Publications website at DOI: 10.1021/acsami.6b02765.

Experimental details, Figures S1−S15, and Table S1 (PDF)

■ AUTHOR INFORMATION

Corresponding Authors

*E-mail: yqlan@njnu.edu.cn.
*E-mail: baojianchun@njnu.edu.cn.
*E-mail: zhkang@suda.edu.cn.

Author Contributions

†K.L. and R.C. contributed equally.

Notes

The authors declare no competing financial interest.

■ ACKNOWLEDGMENTS

This work was financially supported by NSFC (21371099, 21471080, and 21471081), the Jiangsu Specially-Appointed Professor, the NSF of Jiangsu Province of China (BK20130043 and BK20141445), the Natural Science Research of Jiangsu Higher Education Institutions of China (13KJB150021), the Priority Academic Program Development of Jiangsu Higher Education Institutions, and the Foundation of Jiangsu Collaborative Innovation Center of Biomedical Functional Materials.

■ REFERENCES

(1) Bridewell, V. L.; Alam, R.; Karwacki, C. J.; Kamat, P. V. CdSe/CdS Nanorod Photocatalysts: Tuning the Interfacial Charge Transfer Process through Shell Length. *Chem. Mater.* **2015**, *27*, 5064−5071.

(2) Dong, Y.; Choi, J.; Jeong, H.-K.; Son, D. H. Hot Electrons Generated from Doped Quantum Dots via Upconversion of Excitons to Hot Charge Carriers for Enhanced Photocatalysis. *J. Am. Chem. Soc.* **2015**, *137*, 5549−5554.

(3) Hou, Y.; Zuo, F.; Dagg, A.; Feng, P. A Three-Dimensional Branched Cobalt-Doped α-Fe_2O_3 Nanorod/$MgFe_2O_4$ Heterojunction Array as a Flexible Photoanode for Efficient Photoelectrochemical Water Oxidation. *Angew. Chem., Int. Ed.* **2013**, *52*, 1248−1252.

(4) Xie, Y. P.; Yu, Z. B.; Liu, G.; Ma, X. L.; Cheng, H.-M. CdS-mesoporous ZnS Core-shell Particles for Efficient and Stable Photocatalytic Hydrogen Evolution under Visible Light. *Energy Environ. Sci.* **2014**, *7*, 1895−1901.

(5) Xuan, T.-T.; Liu, J.-Q.; Xie, R.-J.; Li, H.-L.; Sun, Z. Microwave-Assisted Synthesis of CdS/ZnS:Cu Quantum Dots for White Light-Emitting Diodes with High Color Rendition. *Chem. Mater.* **2015**, *27*, 1187−1193.

(6) Zhang, Z.; Liu, D.; Li, D.; Huang, K.; Zhang, Y.; Shi, Z.; Xie, R.; Han, M.-Y.; Wang, Y.; Yang, W. Dual Emissive Cu:InP/ZnS/InP/ZnS Nanocrystals: Single-Source "Greener" Emitters with Flexibly Tunable Emission from Visible to Near-Infrared and Their Application in White Light-Emitting Diodes. *Chem. Mater.* **2015**, *27*, 1405−1411.

(7) Yu, J.; Zhang, J.; Jaroniec, M. Preparation and Enhanced Visible-Light Photocatalytic H_2-production Activity of CdS Quantum Dots-sensitized $Zn_{1-x}Cd_xS$ Solid Solution. *Green Chem.* **2010**, *12*, 1611−1614.

(8) McDaniel, H.; Pelton, M.; Oh, N.; Shim, M. Effects of Lattice Strain and Band Offset on Electron Transfer Rates in Type-II Nanorod Heterostructures. *J. Phys. Chem. Lett.* **2012**, *3*, 1094−1098.

(9) Zhang, N.; Yang, M.-Q.; Tang, Z.-R.; Xu, Y.-J. Toward Improving the Graphene−Semiconductor Composite Photoactivity via the Addition of Metal Ions as Generic Interfacial Mediator. *ACS Nano* **2014**, *8*, 623−633.

(10) Li, K.; Chen, R.; Li, S.-L.; Han, M.; Xie, S.-L.; Bao, J.-C.; Dai, Z.-H.; Lan, Y.-Q. Self-assembly of a Mesoporous ZnS/mediating interface/CdS Heterostructure with Enhanced Visible-Light Hydrogen-production Activity and Excellent Stability. *Chem. Sci.* **2015**, *6*, 5263−5268.

(11) Li, Q.; Meng, H.; Zhou, P.; Zheng, Y. Q.; Wang, J.; Yu, J. G.; Gong, J. R. $Zn_{1-x}Cd_xS$ Solid Solutions with Controlled Bandgap and Enhanced Visible-Light Photocatalytic H_2-Production Activity. *ACS Catal.* **2013**, *3*, 882−889.

(12) Li, Q.; Meng, H.; Yu, J. G.; Xiao, W.; Zheng, Y. Q.; Wang, J. Enhanced Photocatalytic Hydrogen-Production Performance of Graphene-$Zn_xCd_{1-x}S$ Composites by Using an Organic S Source. *Chem. - Eur. J.* **2014**, *20*, 1176−1185.

(13) Zhang, J.; Yu, J.; Jaroniec, M.; Gong, J. R. Noble Metal-Free Reduced Graphene Oxide-$Zn_xCd_{1-x}S$ Nanocomposite with Enhanced Solar Photocatalytic H_2-Production Performance. *Nano Lett.* **2012**, *12*, 4584−4589.

(14) del Valle, F.; Ishikawa, A.; Domen, K.; Villoria de la Mano, J. A.; Sánchez-Sánchez, M. C.; González, I. D.; Herreras, S.; Mota, N.; Rivas, M. E.; Álvarez Galván, M. C.; Fierro, J. L. G.; Navarro, R. M. Influence of Zn Concentration in the Activity of $Cd_{1-x}Zn_xS$ Solid Solutions for Water Splitting under Visible Light. *Catal. Today* **2009**, *143*, 51−56.

(15) Al Kuhaimi, S. A.; Tulbah, Z. Structural, Compositional, Optical, and Electrical Properties of Solution-grown $Zn_xCd_{1-x}S$ Films. *J. Electrochem. Soc.* **2000**, *147*, 214−218.

(16) Wang, X.; Liu, G.; Chen, Z.-G.; Li, F.; Lu, G. Q.; Cheng, H.-M. Efficient and Stable Photocatalytic H_2 Evolution from Water Splitting by $(Cd_{0.8}Zn_{0.2})S$ Nanorods. *Electrochem. Commun.* **2009**, *11*, 1174−1178.

(17) Wang, D.-H.; Wang, L.; Xu, A.-W. Room-temperature Synthesis of $Zn_{0.80}Cd_{0.20}S$ Solid Solution with a High Visible-Light Photocatalytic Activity for Hydrogen Evolution. *Nanoscale* **2012**, *4*, 2046−2053.

(18) Liu, J.; Liu, Y.; Liu, N.; Han, Y.; Zhang, X.; Huang, H.; Lifshitz, Y.; Lee, S.-T.; Zhong, J.; Kang, Z. Metal-free Efficient Photocatalyst for Stable Visible Water Splitting via a Two-electron Pathway. *Science* **2015**, *347*, 970−974.

(19) Han, Z.; Chen, G.; Li, C.; Yu, Y.; Zhou, Y. Preparation of 1D Cubic $Cd_{0.8}Zn_{0.2}S$ Solid-solution Nanowires Using Levelling Effect of TGA and Improved Photocatalytic H_2-production Activity. *J. Mater. Chem. A* **2015**, *3*, 1696−1702.

(20) Nien, Y.-T.; Chen, P.-W.; Chen, I.-G. Synthesis and Characterization of $Zn_{1-x}Cd_xS$:Cu, Cl Red Electroluminescent Phosphor Powders. *J. Alloys Compd.* **2008**, *462*, 398−403.

(21) Xie, J.; Zhang, H.; Li, S.; Wang, R.; Sun, X.; Zhou, M.; Zhou, J.; Lou, X. W.; Xie, Y. Defect-Rich MoS_2 Ultrathin Nanosheets with Additional Active Edge Sites for Enhanced Electrocatalytic Hydrogen Evolution. *Adv. Mater.* **2013**, *25*, 5807−5813.

(22) Kibsgaard, J.; Chen, Z.; Reinecke, B. N.; Jaramillo, T. F. Engineering the Surface Structure of MoS_2 to Preferentially Expose Active Edge Sites for Electrocatalysis. *Nat. Mater.* **2012**, *11*, 963−969.

(23) Zhou, D.; Han, B.-H. Graphene-Based Nanoporous Materials Assembled by Mediation of Polyoxometalate Nanoparticles. *Adv. Funct. Mater.* **2010**, *20*, 2717−2722.

(24) Chen, C.-C.; Chang, W.-H.; Yoshimura, K.; Ohya, K.; You, J.; Gao, J.; Hong, Z.; Yang, Y. An Efficient Triple-Junction Polymer Solar Cell Having a Power Conversion Efficiency Exceeding 11%. *Adv. Mater.* **2014**, *26*, 5670−5677.

(25) Jiang, P.; Liu, Q.; Liang, Y. H.; Tian, J. Q.; Asiri, A. M.; Sun, X. P. A Cost-Effective 3D Hydrogen Evolution Cathode with High Catalytic Activity: FeP Nanowire Array as the Active Phase. *Angew. Chem., Int. Ed.* **2014**, *53*, 12855−12859.

DOI: 10.1021/acsami.6b02765
ACS Appl. Mater. Interfaces 2016, 8, 14535−14541

(26) Huang, H. J.; Yang, S. B.; Vajtai, R.; Wang, X.; Ajayan, P. M. Pt-Decorated 3D Architectures Built from Graphene and Graphitic Carbon Nitride Nanosheets as Efficient Methanol Oxidation Catalysts. *Adv. Mater.* **2014**, *26*, 5160−5165.
(27) Li, Q.; Guo, B.; Yu, J.; Ran, J.; Zhang, B.; Yan, H.; Gong, J. R. Highly Efficient Visible-Light-Driven Photocatalytic Hydrogen Production of CdS-Cluster-Decorated Graphene Nanosheets. *J. Am. Chem. Soc.* **2011**, *133*, 10878−10884.
(28) Zong, X.; Yan, H.; Wu, G.; Ma, G.; Wen, F.; Wang, L.; Li, C. Enhancement of Photocatalytic H_2 Evolution on CdS by Loading MoS_2 as Cocatalyst under Visible Light Irradiation. *J. Am. Chem. Soc.* **2008**, *130*, 7176−7177.
(29) Xie, G.; Zhang, K.; Guo, B.; Liu, Q.; Fang, L.; Gong, J. R. Graphene-Based Materials for Hydrogen Generation from Light-Driven Water Splitting. *Adv. Mater.* **2013**, *25*, 3820−3839.
(30) Huang, L.; Wang, X.; Yang, J.; Liu, G.; Han, J.; Li, C. Dual Cocatalysts Loaded Type I CdS/ZnS Core/Shell Nanocrystals as Effective and Stable Photocatalysts for H_2 Evolution. *J. Phys. Chem. C* **2013**, *117*, 11584−11591.
(31) Zhang, J.; Wang, Y.; Jin, J.; Zhang, J.; Lin, Z.; Huang, F.; Yu, J. Efficient Visible-Light Photocatalytic Hydrogen Evolution and Enhanced Photostability of Core/Shell CdS/g-C_3N_4 Nanowires. *ACS Appl. Mater. Interfaces* **2013**, *5*, 10317−10324.
(32) Liu, M.; Li, F.; Sun, Z.; Ma, L.; Xu, L.; Wang, Y. Noble-metal-free Photocatalysts MoS_2-graphene/CdS Mixed Nanoparticles/nanorods Morphology with High Visible Light Efficiency for H_2 Evolution. *Chem. Commun.* **2014**, *50*, 11004−11007.
(33) Wang, Q.; Li, J.; Bai, Y.; Lian, J.; Huang, H.; Li, Z.; Lei, Z.; Shangguan, W. Photochemical Preparation of Cd/CdS Photocatalysts and Their Efficient Photocatalytic Hydrogen Production under Visible Light Irradiation. *Green Chem.* **2014**, *16*, 2728−2735.
(34) Liu, S. Q.; Zhang, N.; Tang, Z. R.; Xu, Y. J. Synthesis of One-Dimensional CdS@TiO_2 Core-Shell Nanocomposites Photocatalyst for Selective Redox: The Dual Role of TiO_2 Shell. *ACS Appl. Mater. Interfaces* **2012**, *4*, 6378−6385.
(35) Li, K.; Chen, R.; Li, S.-L.; Xie, S.-L.; Cao, X.-L.; Dong, L.-Z.; Bao, J.-C.; Lan, Y.-Q. Engineering the Morphology and Configuration of Ternary Heterostructures for Improving Their Photocatalytic Activity. *ACS Appl. Mater. Interfaces* **2016**, *8*, 4516−4522.
(36) Zhang, J.; Wang, L.; Liu, X.; Li, X. a.; Huang, W. High-performance CdS-ZnS Core-shell Nanorod Array Photoelectrode for Photoelectrochemical Hydrogen Generation. *J. Mater. Chem. A* **2015**, *3*, 535−541.
(37) Peng, W. Q.; Cong, G. W.; Qu, S. C.; Wang, Z. G. Synthesis and Photoluminescence of ZnS:Cu Nanoparticles. *Opt. Mater.* **2006**, *29*, 313−317.
(38) Chawla, A. K.; Singhal, S.; Nagar, S.; Gupta, H. O.; Chandra, R. Study of Composition Dependent Structural, Optical, and Magnetic Properties of Cu-doped $Zn_{1-x}Cd_xS$ Nanoparticles. *J. Appl. Phys.* **2010**, *108*, 123519.

DOI: 10.1021/acsami.6b02765
ACS Appl. Mater. Interfaces 2016, 8, 14535−14541